Supporting Information for

ORIGINAL ARTICLE

Acid-switchable nanoparticles induce self-adaptive aggregation for enhancing antitumor immunity of natural killer cells

Xiangshi Sun[a,b], Xiaoxuan Xu[b], Jue Wang[b], Xinyue Zhang[f], Zitong Zhao[b], Xiaochen Liu[b], Guanru Wang[b], Lesheng Teng[d], Xia Chen[a,*], Dangge Wang[b,c,*], Yaping Li[b,e,f,*]

[a]*Department of Pharmacology, College of Basic Medical Sciences, Jilin University, Changchun 130021, China*

[b]*State Key Laboratory of Drug Research & Center of Pharmaceutics, Shanghai Institute of Materia Medica, Chinese Academy of Sciences, Shanghai 201203, China*

[c]*Yantai Key Laboratory of Nanomedicine & Advanced Preparations, Yantai Institute of Materia Medica, Yantai 264000, China*

[d]*School of Life Sciences, Jilin University, Changchun 130012, China*

[e]*Shandong Laboratory of Yantai Drug Discovery, Bohai Rim Advanced Research Institute for Drug Discovery, Yantai 264000, China*

[f]*School of Chinese Materia Medica, Nanjing University of Chinese Medicine, Nanjing 210023, China*

*Corresponding authors.

E-mail addresses: chenxjluedu@163.com (Xia Chen), dgwang@simm.ac.cn (Dangge Wang), ypli@simm.ac.cn (Yaping Li).

Table S1 Composition of control and treated nanoparticles.

Need heading	NaAlg	CaCO$_3$	Galunisertib	IL-15
Gal/IL-15			√	√
Gal/IL-15@Ca		√	√	√
Gal@CaLN	√	√	√	
IL-15@CaLN	√	√		√
Gal/IL-15@LN	√		√	√

| Gal/IL-15@CaLN | √ | √ | √ | √ |

Table S2 Encapsulation efficiency (EE) and loading capability (LC) of galunisertib and IL-15 of Gal/IL-15@CaLN and Gal/IL-15@LN. Data were expressed as mean ± SD ($n = 3$).

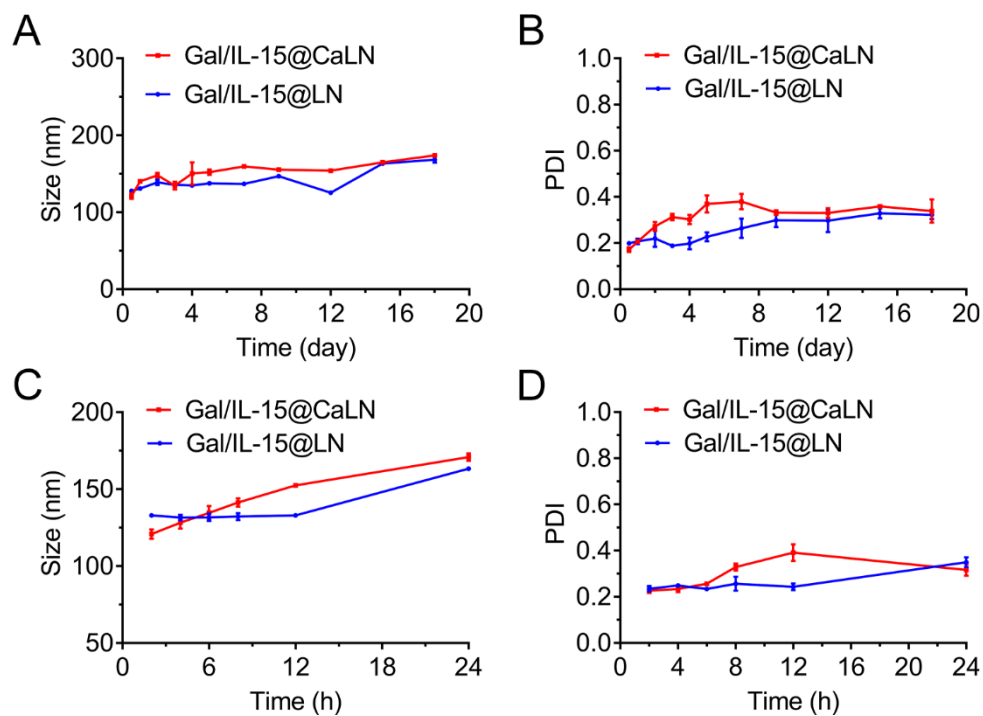|		Gal/IL-15@CaLN	Gal/IL-15@LN
Galunisertib	EE(%)	77.9 ± 0.2	81.6 ± 0.1
	LC(%)	4.3 ± 0.01	4.5 ± 0.01
IL-15	EE(%)	88.0 ± 1.6	91.9 ± 1.4
	LC	0.98 ± 0.02 μg/10 mg	1.02 ± 0.02 μg/10 mg

Figures

Figure S1 (A) Hydrodynamic size and (B) PDI of Gal/IL-15@CaLN and Gal/IL-15@LN after dispersed in PBS for desired duration. (C) Hydrodynamic size and (D) PDI of Gal/IL-15@CaLN and Gal/IL-15@LN in PBS with 10% FBS. Data were expressed as mean ± SD (n = 3).
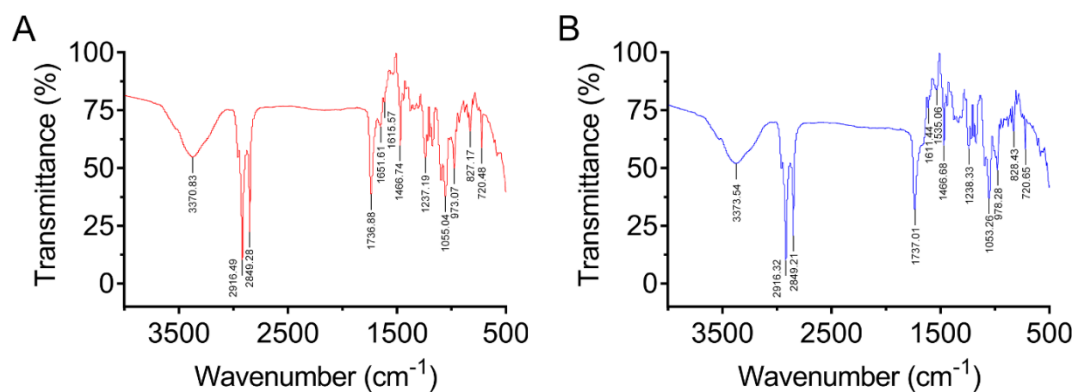

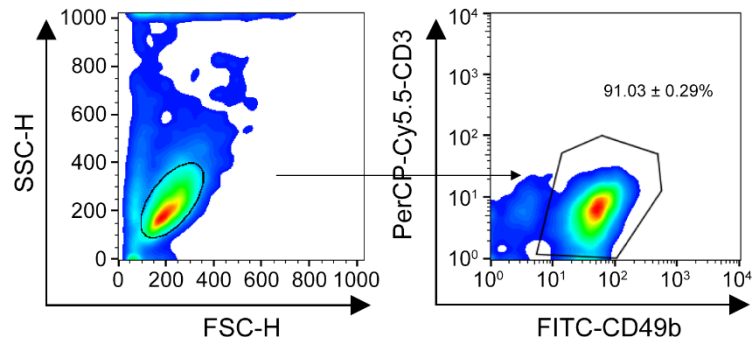**Figure S2** FTIR spectrum of (A) Gal/IL-15@CaLN, (B) Gal/IL-15@CaLN in acidic buffer.

Figure S3 Flow cytometry analysis of purity of NK cells (gating on CD3⁻CD49b⁺ cells) separated from BALB/c mouse spleens and afterwards purified by flow cytometer. Data were expressed as mean ± SD ($n = 3$).
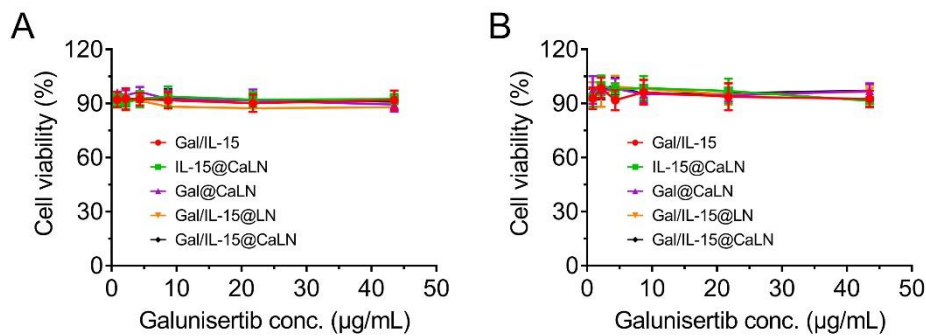

Figure S4 Cell viability of (A) NK cells and (B) CT26 cells after treated by various treatments. The concentration gradient of galunisertib varied from 0.87 to 43.5 μg/mL, and that of IL-15 was 2–100 ng/mL. Data were expressed as mean ± SD ($n = 6$).
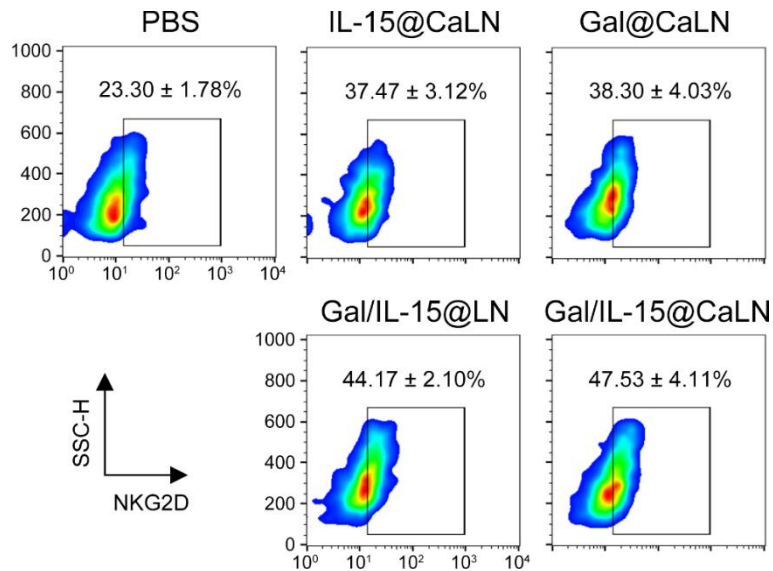

Figure S5 NKG2D expression in NK cells evaluated by flow cytometry. NK cells (2×10^5) were incubated with CT26 cells (2×10^5) for 24 h and then treated by various treatments (PBS, IL-15@CaLN, Gal@CaLN, Gal/IL-15@LN, Gal/IL-15@CaLN) at identical 20 ng/mL IL-15 or/and 8.7 μg/mL galunisertib for 12 h, following by staining with anti-NKG2D-APC antibody. Data were expressed as mean ± SD ($n = 3$).
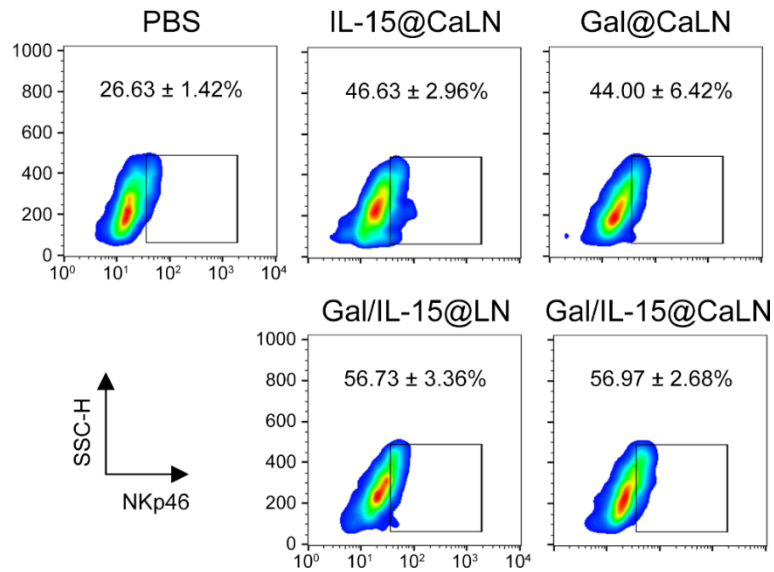
Figure S6 NKp46 expression in NK cells evaluated by flow cytometry. NK cells (2×10^5) were incubated with CT26 cells (2×10^5) for 24 h and then treated by various treatments (PBS, IL-15@CaLN, Gal@CaLN, Gal/IL-15@LN, Gal/IL-15@CaLN) at identical 20 ng/mL IL-15 or/and 8.7 µg/mL galunisertib for 12 h, followed by staining with anti-NKp46-PE antibody. Data were expressed as mean ± SD ($n = 3$).
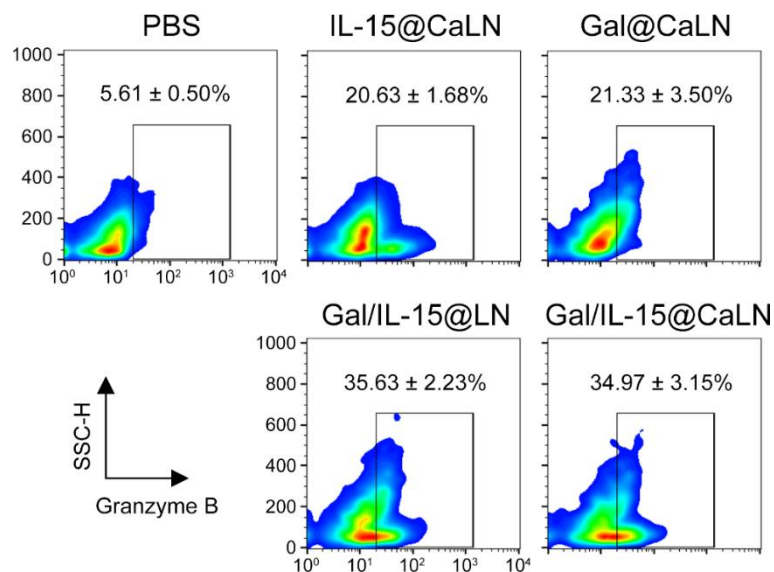

Figure S7 Granzyme B expression in NK cells evaluated by flow cytometry. NK cells (2×10^5) were incubated with CT26 cells (2×10^5) for 24 h and then treated by various treatments (PBS, IL-15@CaLN, Gal@CaLN, Gal/IL-15@LN, Gal/IL-15@CaLN) at identical 20 ng/mL IL-15 or/and 8.7 µg/mL galunisertib for 12 h, followed by staining with anti-Granzyme B-Alexa Fluor 647 antibody. Data were expressed as mean ± SD ($n = 3$).

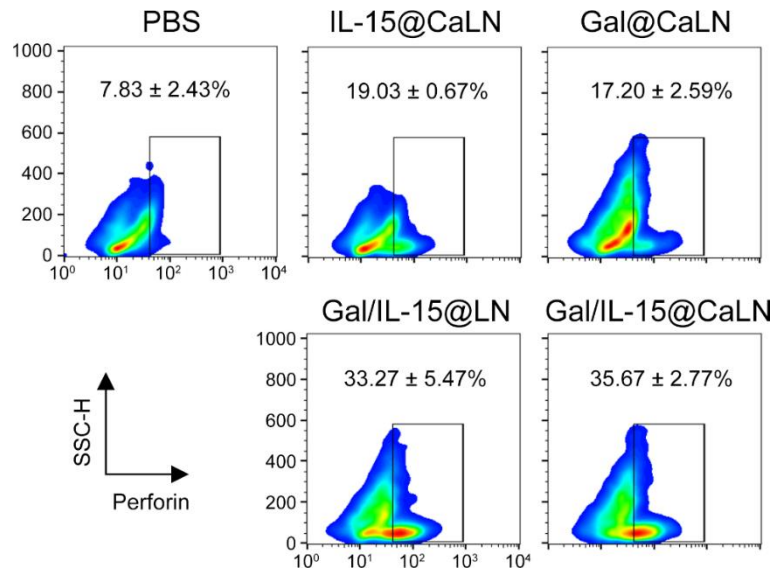**Figure S8** Perforin expression in NK cells evaluated by flow cytometry. NK cells (2×10^5) were incubated with CT26 cells (2×10^5) for 24 h and then treated by various treatments (PBS, IL-15@CaLN, Gal@CaLN, Gal/IL-15@LN, Gal/IL-15@CaLN) at identical 20 ng/mL IL-15 or/and 8.7 μg/mL galunisertib for 12 h, followied by staining with anti-Perforin-PE antibody. Data were expressed as mean $\pm$ SD ($n = 3$).
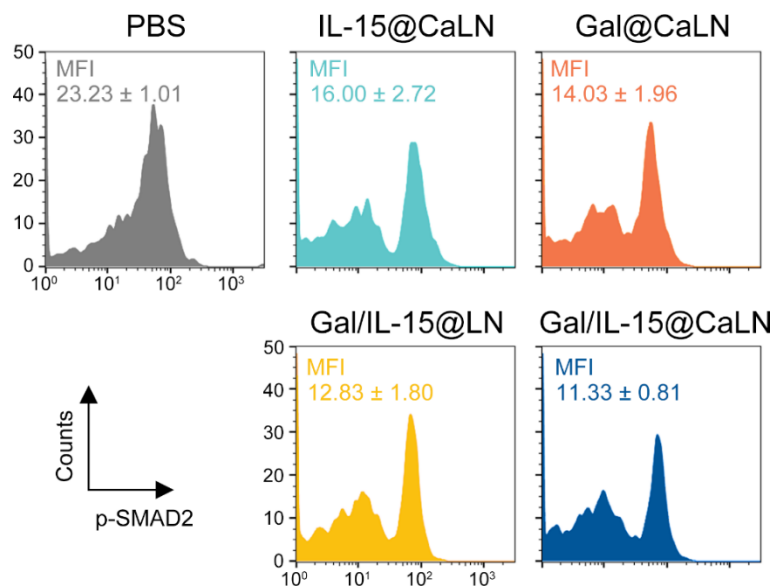

Figure S9 p-SMAD2 expression in NK cells evaluated by flow cytometry. NK cells (2×10^5) were incubated with CT26 cells (2×10^5) for 24 h and then treated by various treatments (PBS, IL-15@CaLN, Gal@CaLN, Gal/IL-15@LN, Gal/IL-15@CaLN) at identical 20 ng/mL IL-15 or/and 8.7 μg/mL galunisertib for 12 h, followed by staining with anti-p-SMAD2 primary antibody and corresponding PE-conjugated secondary antibody. Data were expressed as mean $\pm$ SD ($n = 3$).
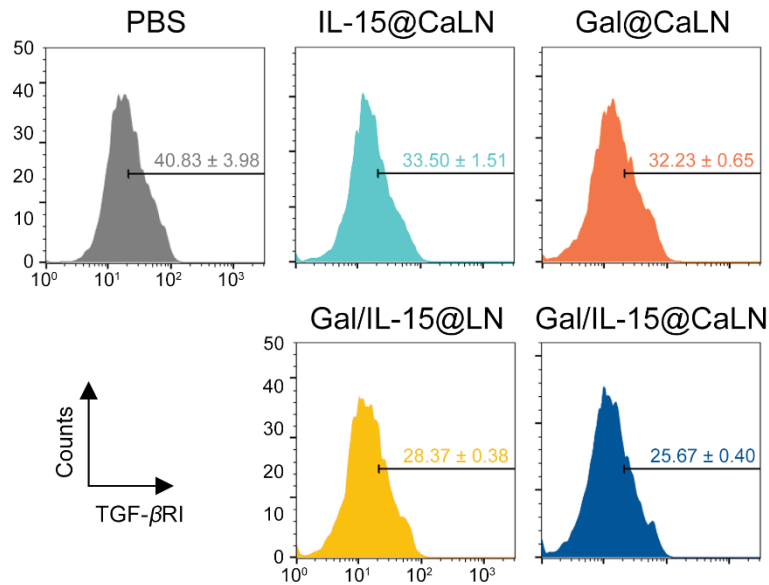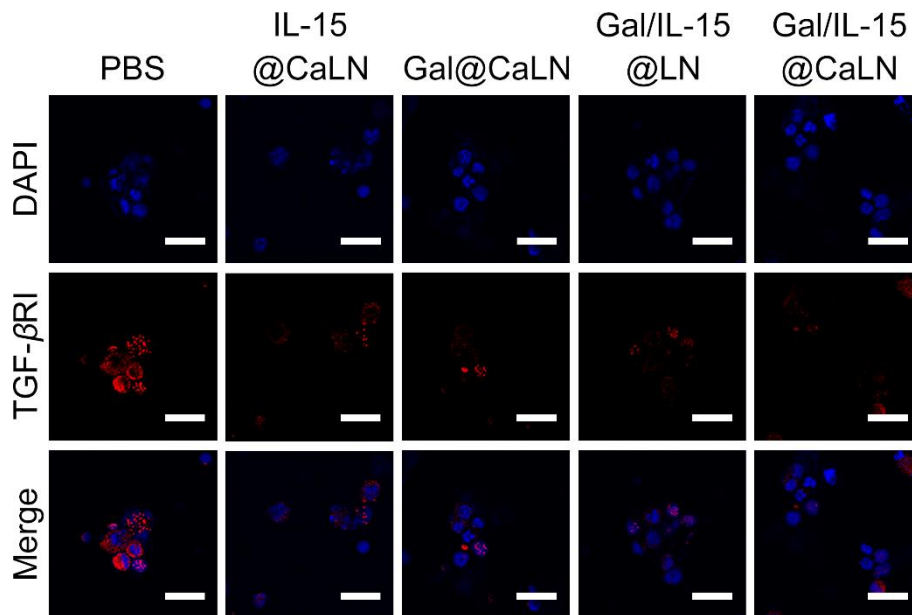
Figure S10 TGF-βRI expression in NK cells evaluated by flow cytometry. NK cells (2×10^5) were incubated with CT26 cells (2×10^5) for 24 h and then treated by various treatments (PBS, IL-15@CaLN, Gal@CaLN, Gal/IL-15@LN, Gal/IL-15@CaLN) at identical 20 ng/mL IL-15 or/and 8.7 μg/mL galunisertib for 12 h, followed by staining with anti-TGF-βRI primary antibody and corresponding PE-conjugated secondary antibody. Data were expressed as mean ± SD ($n = 3$).

Figure S11 TGF-βRI expression in NK cells evaluated by CLSM. NK cells (2×10^5) were incubated with CT26 cells (2×10^5) for 24 h and then treated by various treatments (PBS, IL-15@CaLN, Gal@CaLN, Gal/IL-15@LN, Gal/IL-15@CaLN) at identical 20 ng/mL IL-15 or/and 8.7 μg/mL galunisertib for 12 h, followed by staining with anti-TGF-βRI primary antibody and corresponding Alexa Fluor 647-conjugated secondary antibody (Blue signals: DAPI; red signals: TGF-βRI). Scale bar, 25 μm.
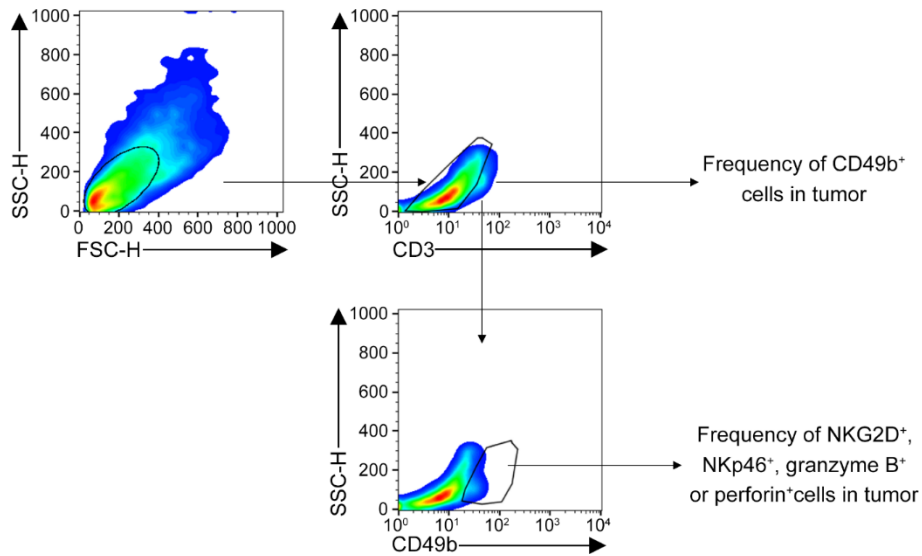
Figure S12 Gating strategies for identification of intratumoral NK cells (gating on CD3$^-$CD49b$^+$ cells), NKG2D$^+$ NK cells (gating on CD3$^-$CD49b$^+$NKG2D$^+$ cells), NKp46$^+$ NK cells (gating on CD3$^-$CD49b$^+$NKp46$^+$ cells), Granzyme B$^+$ NK cells (gating on CD3$^-$CD49b$^+$Granzyme B$^+$ cells), and Perforin$^+$ NK cells (gating on CD3$^-$CD49b$^+$Perfotin$^+$ cells) in CT26 tumor-bearing immune-deficient BALB/c-nu mice.
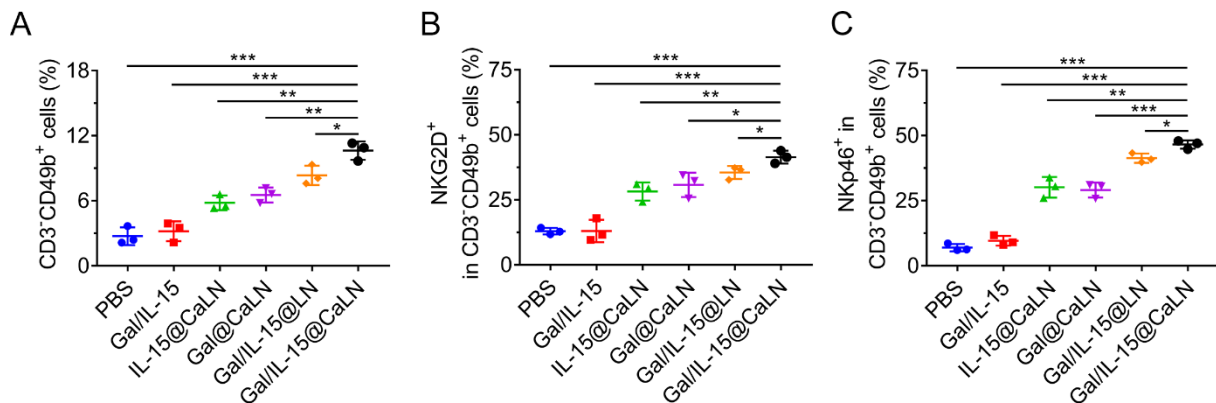

Figure S13 Frequency of intratumoral NK cell populations in CT26 tumor-bearing BALB/c-nu mice. (A) Frequency of NK cells (gating on CD3$^-$CD49b$^+$ cells). (B) Frequency of NKG2D$^+$ NK cells (gating on CD3$^-$CD49b$^+$NKG2D$^+$ cells). (C) Frequency of NKp46$^+$ NK cells (gating on CD3$^-$CD49b$^+$NKp46$^+$ cells). Data were expressed as mean ± SD. The statistical significance was displayed by two-sided unpaired Student's *t*-test. ($^*P < 0.05$, $^{**}P < 0.01$, $^{***}P < 0.001$) ($n = 3$).
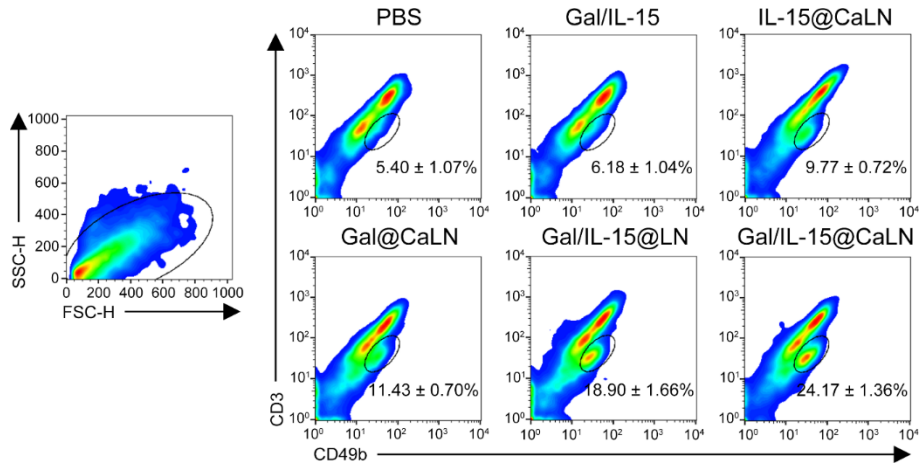
Figure S14 Gating strategies and frequency of intratumoral NK cell populations (gating on CD3$^-$CD49b$^+$ cells) in CT26 tumor-bearing BALB/c-ic mice. Data were expressed as mean ± SD (n = 3).
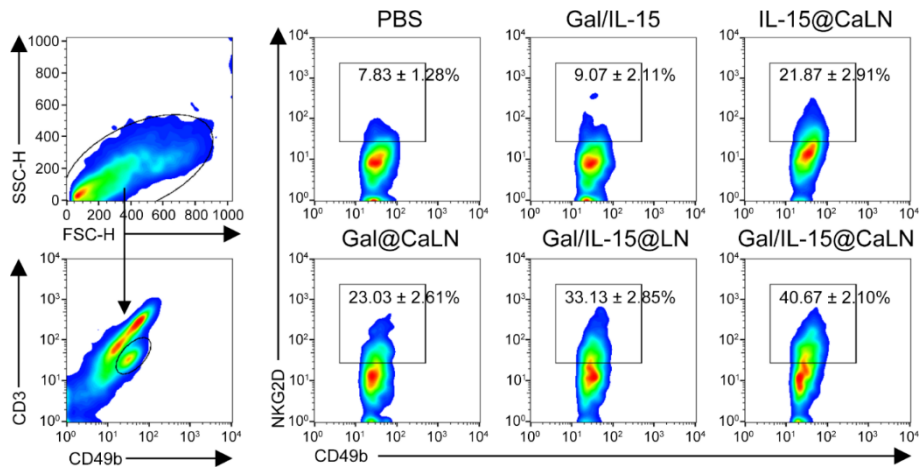

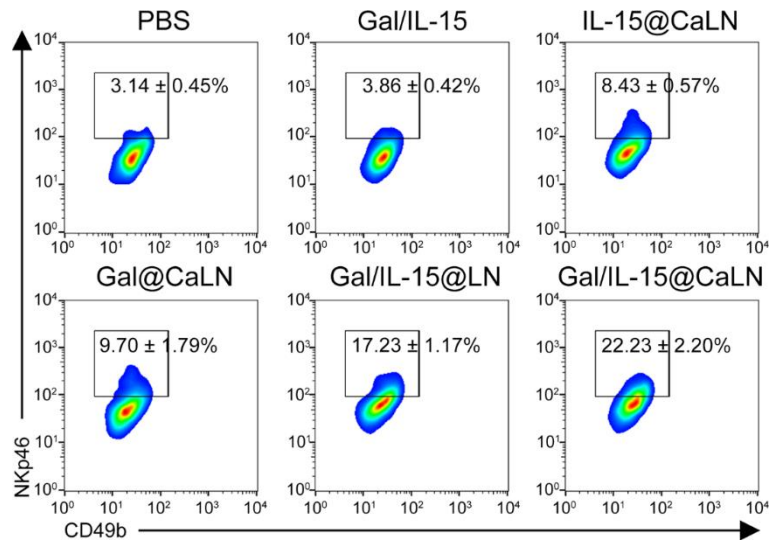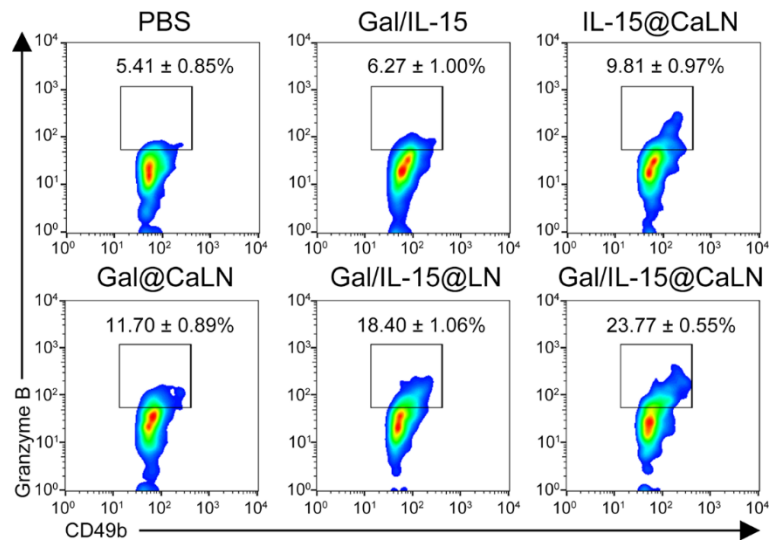**Figure S15** Gating strategies and frequency of intratumoral NKG2D$^+$ NK cell populations (gating on CD3$^-$CD49b$^+$NKG2D$^+$ cells) in CT26 tumor-bearing BALB/c-ic mice. Data were expressed as mean ± SD (n = 3).
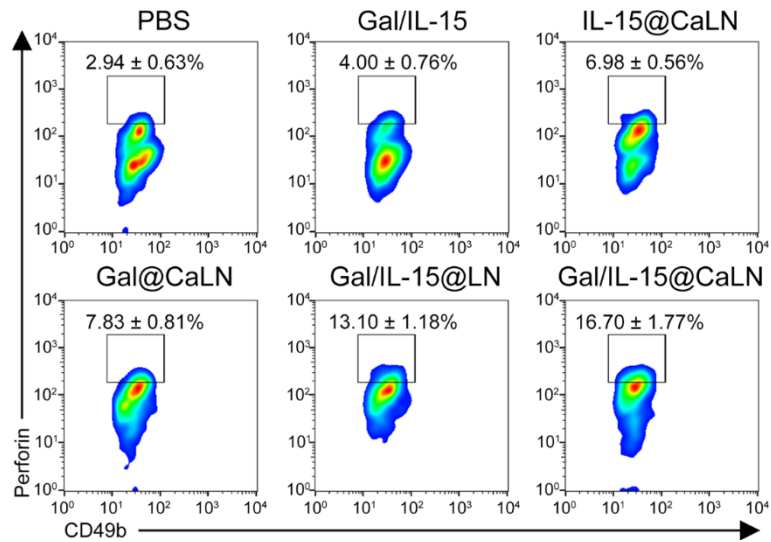
Figure S16 Frequency of intratumoral NKp46$^+$ NK cell populations (gating on CD3$^-$CD49b$^+$NKp46$^+$ cells) in CT26 tumor-bearing BALB/c-ic mice. Data were expressed as mean $\pm$ SD ($n = 3$).

Figure S17 Frequency of intratumoral Granzyme B$^+$ NK cell populations (gating on CD3$^-$CD49b$^+$Granzyme B$^+$ cells) in CT26 tumor-bearing BALB/c-ic mice. Data were expressed as mean $\pm$ SD ($n = 3$).

Figure S18 Frequency of intratumoral Perforin$^+$ NK cell populations (gating on CD3$^-$CD49b$^+$Perforin$^+$ cells) in CT26 tumor-bearing BALB/c-ic mice. Data were expressed as mean ± SD ($n = 3$).
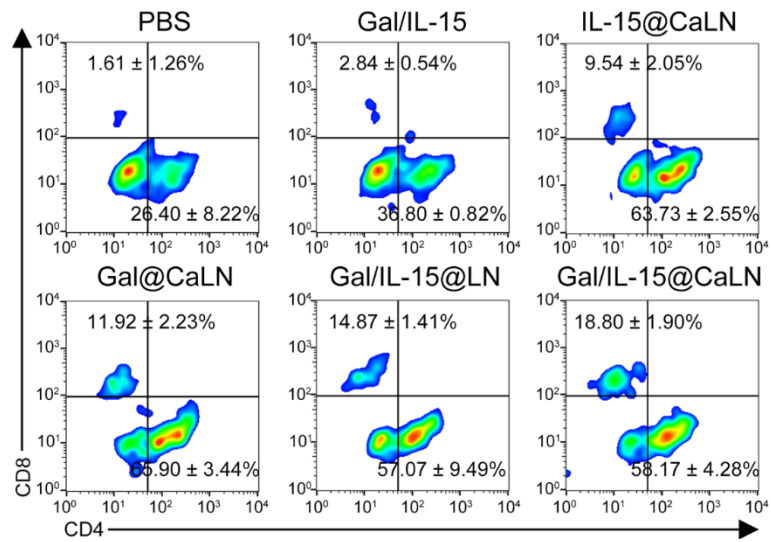

Figure S19 Frequency of intratumoral CD8$^+$ T cell (gating on CD3$^+$CD8$^+$ cells) and CD4$^+$ T cell populations (gating on CD3$^+$CD4$^+$ cells) in CT26 tumor-bearing BALB/c-ic mice. Data were expressed as mean ± SD ($n = 3$).
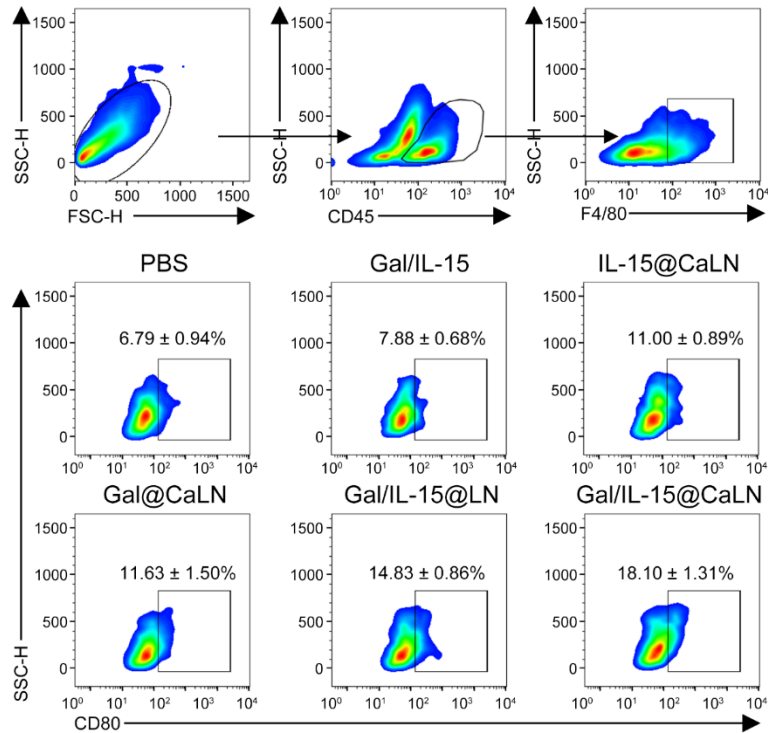
Figure S20 Gating strategies and frequency of intratumoral M1 macrophage populations (gating on CD45$^+$F4/80$^+$CD80$^+$ cells) in CT26 tumor-bearing BALB/c-ic mice. Data were expressed as mean ± SD (n = 3).
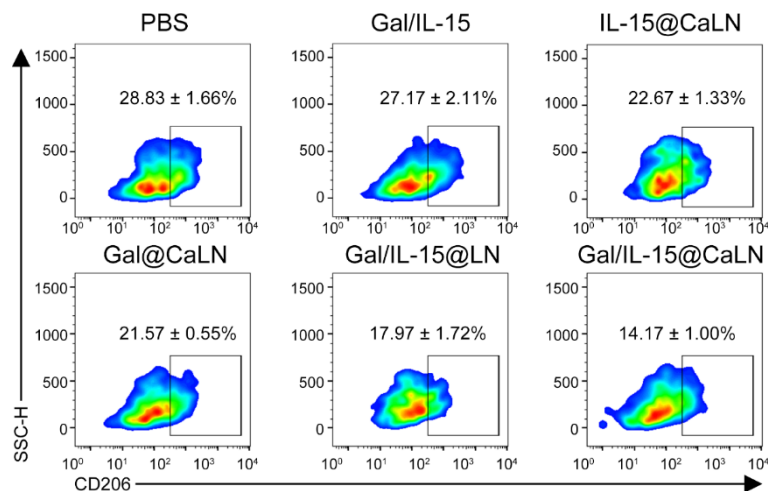

Figure S21 Frequency of intratumoral M2 macrophage populations (gating on CD45$^+$F4/80$^+$CD206$^+$ cells) in CT26 tumor-bearing BALB/c-ic mice. Data were expressed as mean ± SD (n = 3).
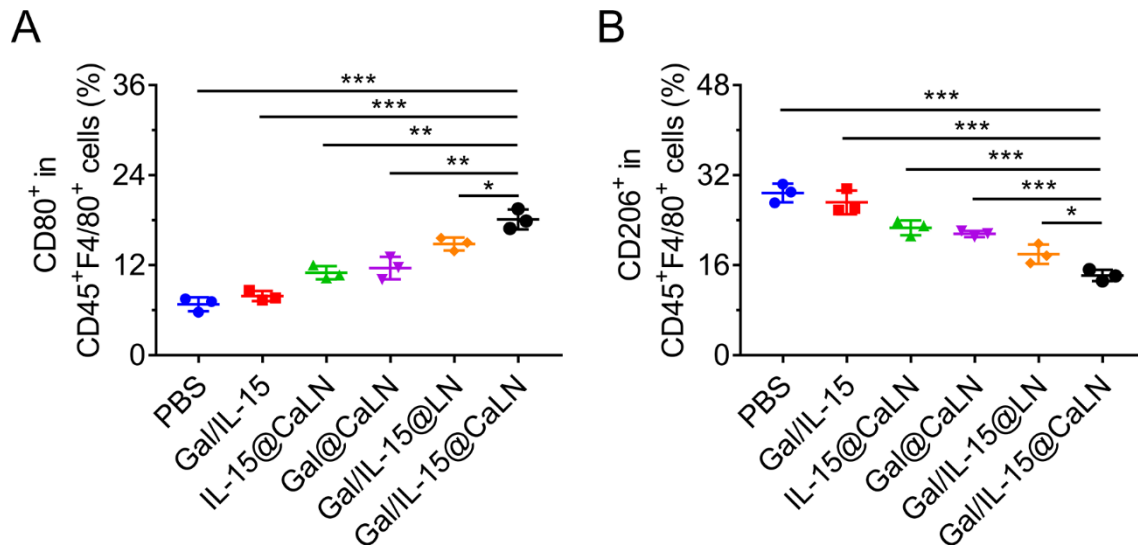
Figure S22 Frequency of intratumoral macrophage populations in CT26 tumor-bearing BALB/c-ic mice. (A) Frequency of M1 macrophage populations (gating on CD45$^+$F4/80$^+$CD80$^+$ cells). (B) Frequency of M2 macrophage populations (gating on CD45$^+$F4/80$^+$CD206$^+$ cells). Data were expressed as mean ± SD (n = 3). The statistical significance was displayed by two-sided unpaired Student's t-test. ($^*P < 0.05$, $^{**}P < 0.01$, $^{***}P < 0.001$).
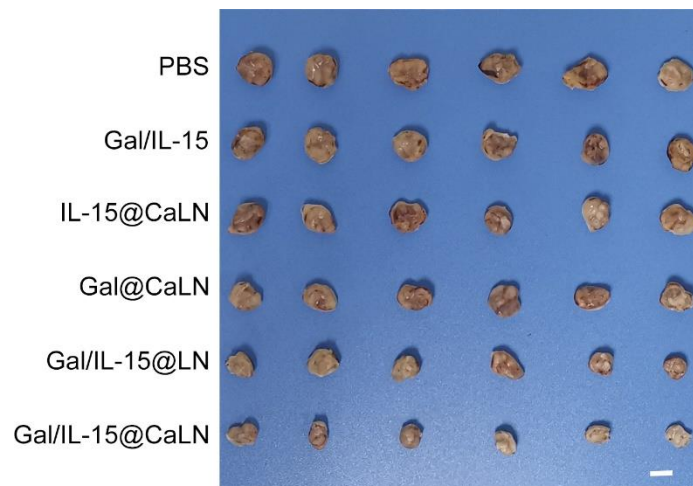

Figure S23 Photographs of tumors at Day 14 of antitumor study in CT26 tumor-bearing BALB/c-nu mice (n = 6). Scale bar, 1 cm.
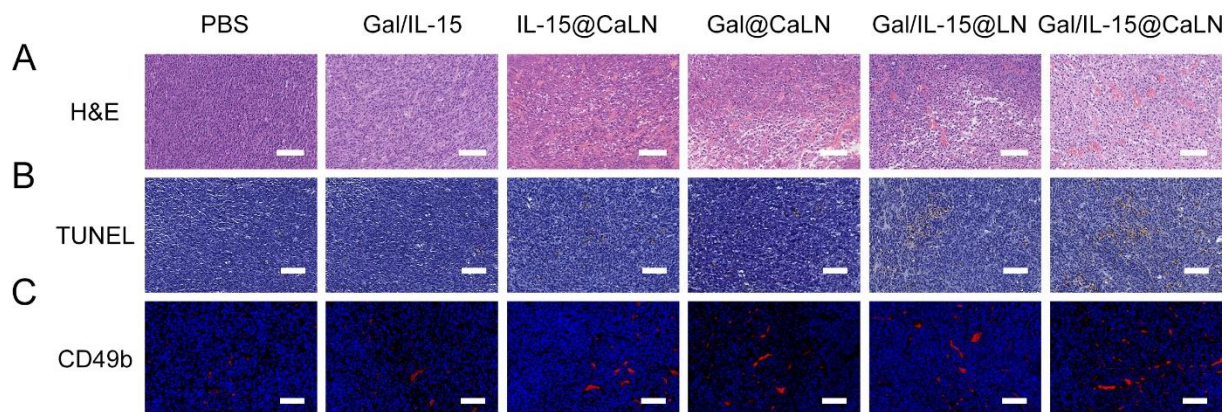
Figure S24 Tumor section assays at Day 14 of antitumor study in CT26 tumor-bearing BALB/c-nu mice. (A) H&E staining. (B) TUNEL staining. (C) The infiltration of NK cells characterized as CD49b$^+$ cells (Blue signals: DAPI; red signals: CD49b). Scale bar, 100 μm.
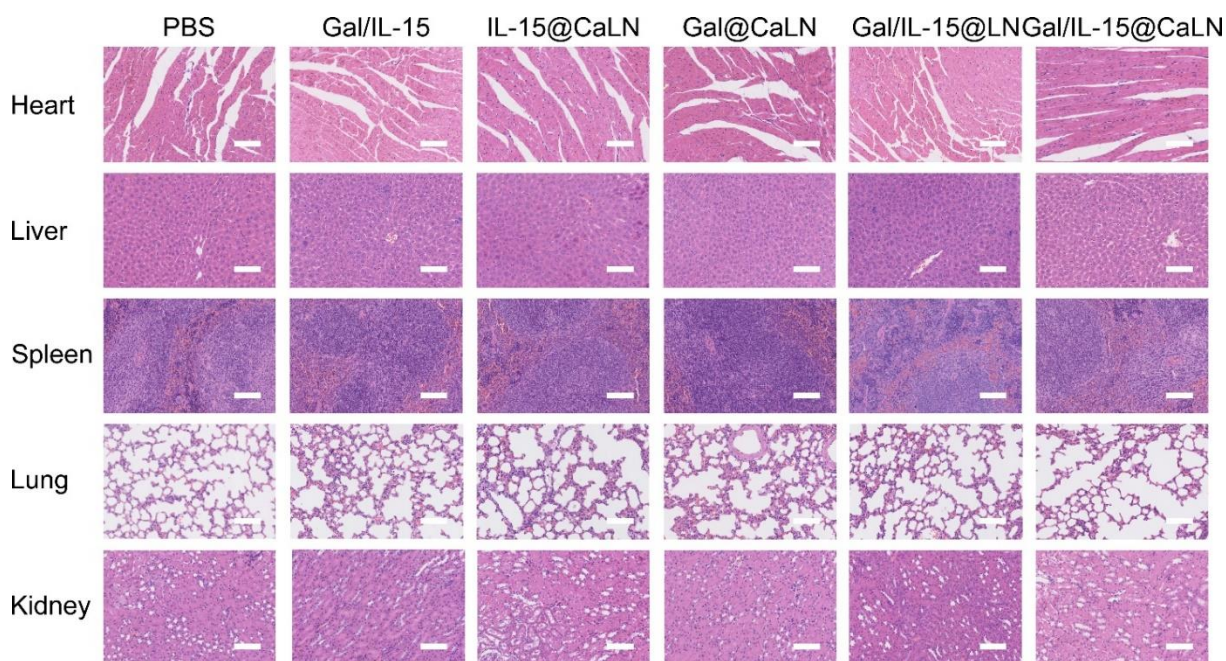

Figure S25 H&E staining of major organs (heart, liver, spleen, lung, kidney) at Day 14 of antitumor study in CT26 tumor-bearing BALB/c-nu mice. Scale bar, 100 μm.
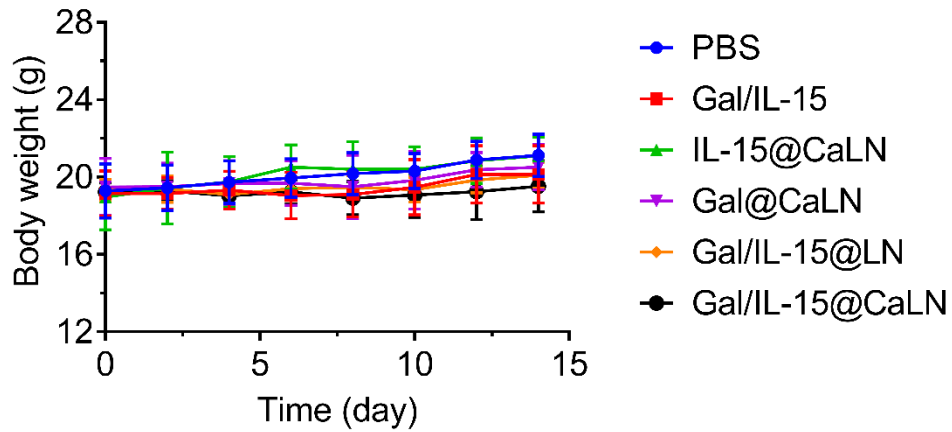
Figure S26 Body weight change monitored every two days during the antitumor study in CT26 tumor-bearing BALB/c-nu mice. Data were expressed as mean ± SD ($n = 6$).
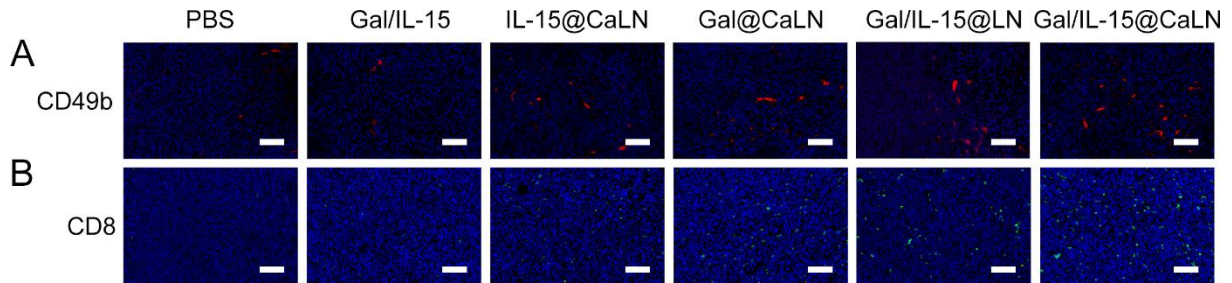

Figure S27 Immunofluorescence staining of tumor sections at Day 16 of antitumor study in CT26 tumor-bearing BALB/c-ic mice. (A) The infiltration of NK cells characterized as CD49b+ cells (Blue signals: DAPI; red signals: CD49b). (B) The infiltration of CD8+ T cells characterized as CD8+ cells (Blue signals: DAPI; green signals: CD8). Scale bar, 100 μm.
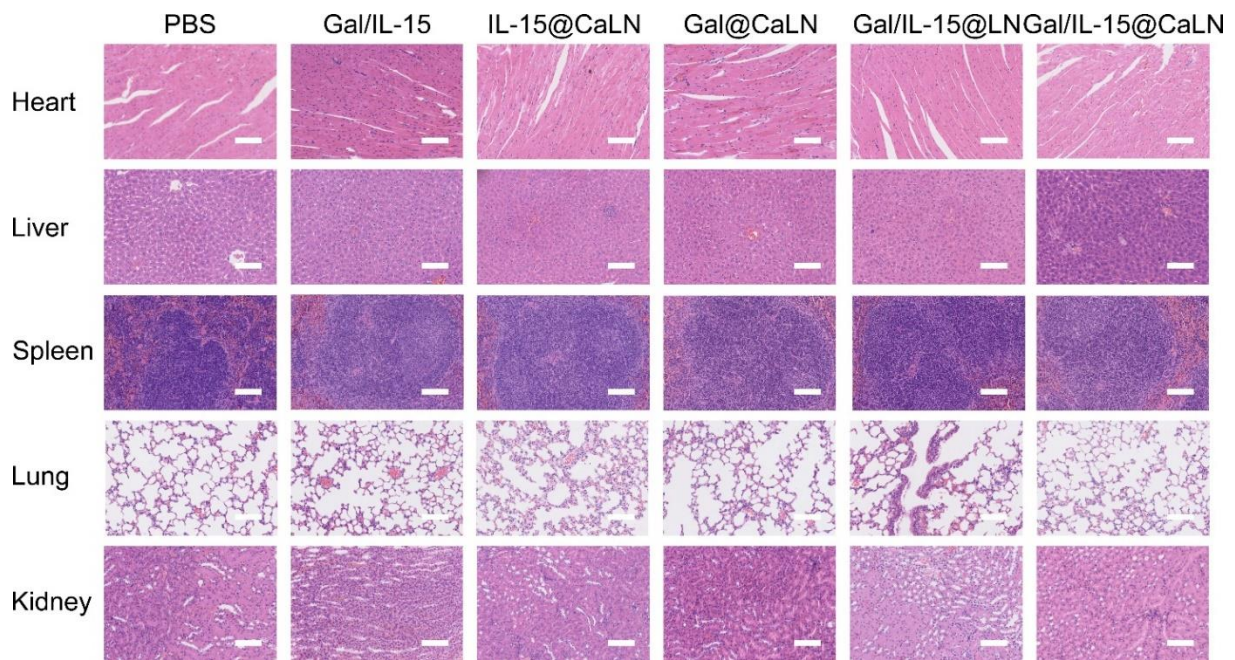
Figure S28 H&E staining of major organs (heart, liver, spleen, lung, kidney) at Day 16 of antitumor study in CT26 tumor-bearing BALB/c-ic mice. Scale bar, 100 μm.
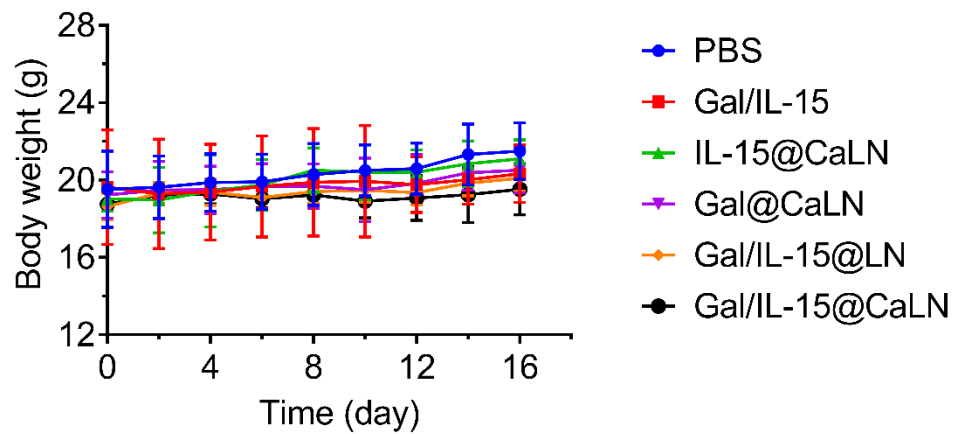

Figure S29 Body weight change monitored every two days during the antitumor study in CT26 tumor-bearing BALB/c-ic mice. Data were expressed as mean ± SD ($n = 6$).